Materials Today Communications 36 (2023) 106496

Contents lists available at ScienceDirect

Materials Today Communications

journal homepage: www.elsevier.com/locate/mtcomm

Adsorption and migration of Cs and Na ions in geopolymers and zeolites

Eduardo Duque-Redondo [a,b,*], Kazuo Yamada [c], Enrico Masoero [b,d], Jorge Bañuelos Prieto [a], Hegoi Manzano [e]

[a] Department of Physical Chemistry, University of the Basque Country UPV/EHU, Aptdo. 664, 48080 Bilbao, Spain
[b] School of Engineering, Newcastle University, Newcastle upon Tyne NE17RU, UK
[c] Fukushima Branch, National Institute for Environmental Studies, Miharu, Tamura, Fukushima 963-7700, Japan
[d] School of Engineering, Cardiff University, Cardiff CF24 3AA, UK
[e] Department of Physics, University of the Basque Country UPV/EHU, Aptdo. 664, 48080 Bilbao, Spain

ARTICLE INFO

Keywords:
Molecular dynamics
Cesium
Sodium
Adsorption
Geopolymer
Zeolite
Immobilization

ABSTRACT

Geopolymers may provide a more sustainable alternative to Portland Cement for various possible applications. Geopolymers have attracted particular interest for the immobilization of pollutants, owing to their high adsorption capacity, high thermal and chemical resistance, and low leachability. However, practical implementation is currently hindered by a limited understanding of how adsorption processes occur in geopolymers, and how they can be engineered to optimize the incorporation of pollutants and avoid their release. In this work, Molecular Dynamics simulations provide insights into these processes at the atomic scale, studying the role of host material composition and structure in the immobilization of Na and Cs ions. The simulations reveal that the most stable configurations for these ions are near the center of 6- and 8-membered aluminosilicate rings, where the coordination with the geopolymer is maximum. Higher contents of Al and degrees of crystallinity are found to yield more stable configurations for Cs ions, with more favorable adsorption enthalpies and lower diffusion coefficients. The comparison of different crystalline zeolite structures reveals that the framework of sodalite, used as the baseline to develop model geopolymer structures, is the most suitable for the immobilization of Cs since there are no channels and it is formed by small 4- and 6-member, all preventing Cs ions from escaping the cavities.

1. Introduction

The production of cement and concrete has a high carbon footprint due to the limestone calcination process and the use of fossil fuels to reach the high temperatures required to produce clinker. It is estimated that the production of 1 tonne of Portland Cement (PC) releases nearly another tonne of CO_2 and, due to vast global consumption of cement (the most used man-made material [1]), the cement industry is responsible for about 8% of the anthropogenic CO_2 emissions [2]. Thus, there is a strong interest in developing more sustainable alternatives to PC [3]. Geopolymers have emerged as a possible, more sustainable alternative to PC since these materials have shown comparable strength to PC [4–6] and good durability, sometimes even better than that of PC [7,8], while their production entails significantly fewer CO_2 emissions due to the absence of decarbonization processes and lower processing temperatures [9].

Geopolymers are formed by the alkali activation of a finely ground precursor [10]. The geopolymerization process commences with the dissolution of the alkali activator in water, mainly sodium hydroxide (NaOH), potassium hydroxide (KOH), sodium silicate (Na_2SiO_3) and potassium silicate (K_2SiO_3) [11], followed by the progressive release into the solution of silicates and aluminates from the precursor, usually kaolinite, feldspar, or industrial solid residues such as fly ash, metallurgical slag, or mining wastes. This leads to the polymerization of the aluminosilicates, resulting in a gel structure with a three-dimensional network of aluminate and silicate tetrahedra, and alkali cations sitting in its pores to balance the excess of negative charge from tetracoordinated Al. At the macroscale, this polymerization process leads to a paste setting and gaining mechanical strength, akin to what takes place during the hydration of PC, although the underlying chemistry of the reactants and products fundamentally differs from that of PC systems. As in PC, the final properties of the geopolymers can vary considerably depending on their composition; for example, there is a nonlinear dependence of porosity [11–14] and strength [15,16] with the Si/Al ratio, with the best

* Corresponding author at: Department of Physical Chemistry, University of the Basque Country UPV/EHU, Aptdo. 664, 48080 Bilbao, Spain.
E-mail address: eduardo.duque@ehu.eus (E. Duque-Redondo).

https://doi.org/10.1016/j.mtcomm.2023.106496
Received 31 January 2023; Received in revised form 2 June 2023; Accepted 20 June 2023
Available online 22 June 2023

performance typically achieved between 1.4 and 2 [17,18].

The properties of geopolymers make them suitable for various applications, also beyond construction. In particular, the use of geopolymers for the immobilization and solidification of radioactive materials has attracted much attention due to their intrinsic high thermal and chemical resistance [19,20], low leachability [21,22], high adsorption capacity, and feasible cost [23–25]. Experiments have proven that the retention of different hazardous and radioactive wastes, such as Sr and Cs, is more effective in geopolymers than in PC, which is also widely used for the encapsulation of contaminants [24,26–33]. This good performance of geopolymers is attributed to the presence of close cage cavities at the nanometer level, their dense three-dimensional structure, and their high capacity to form strong chemical bonds with the contaminants; similar to zeolites, which have been extensively used for the immobilization of radioisotopes [34–44]. The adsorption capacity of geopolymers is strongly influenced by their composition since low Si/Al ratios entail more tetracoordinated aluminates, whose net negative charge attracts the cations in solution, including positively charged radionuclides, thus increasing their retention [12]. Other factors also impact the immobilization performance [12], e.g. the size and charge of the ions to be confined, the size of the aluminosilicate rings in the molecular structure of the geopolymer, and the charge heterogeneity. Indeed, in zeolites, it is established that their framework and composition determine the selectivity and adsorption capacity towards different heavy metals or radionuclides [45–47].

The potential use of geopolymers for immobilization is particularly interesting for radiocesium, ^{137}Cs, which is one of the most hazardous radioisotopes in spent nuclear fuel due to a long half-life of more than 30 years and a high specific radioactivity [48–51]. Indeed, radiocesium can be tightly docked at the center of 8-membered aluminosilicate rings due to its size [39,41,52]. However, it is still unclear how the composition and nanostructural disorder of geopolymers may impact the mechanisms of adsorption and migration for this contaminant. Understanding these mechanisms at the atomic scale is the first in a rational approach for optimizing the composition and structure of geopolymer, to achieve maximum retention and minimum migration of Cs ions. Atomistic simulations may help shed light on these fundamental mechanisms.

In this work, we employed molecular dynamics (MD) simulations to investigate the adsorption and migration of Cs ions in geopolymers with three different levels of structural order originally developed in ref [53]: (i) fully crystalline, based on the ordered zeolitic structure of sodalite, (ii) fully amorphous, based on the very disordered structure of silica glass, and (iii) defective, viz. intermediate between the two previous cases. Four different compositions of the geopolymers were considered, with Si/Al ratios between 1.4 and 2.0, a (Na+Cs)/Al ratio of 1, and a Cs/Na ratio of 0.5. In addition, we have analyzed four zeolites, with the same compositions as the geopolymers but different crystalline frameworks: (i) sodalite (SOD, equivalent to the crystalline geopolymer), (ii) chabazite (CHA), (iii) mordenite (MOR), and (iv) clinoptilolite (HEU, heulandite framework). In this way, the adsorption capacity of geopolymers can be compared with that of zeolites that have been successfully employed for Cs immobilization. Indeed, the selected zeolites exhibit high adsorption capacity and selectivity towards Cs [54–57]. The adsorption and migration of Na ions, which are typically present in geopolymers and zeolites, were also analyzed since they might affect Cs uptake by occupying and/or competing for the adsorption sites. The efficiency of the immobilization of Cs and Na is investigated by analyzing their coordination with the geopolymers, the lifetime of those interactions, and the adsorption enthalpies, while the migration of the Cs and Na ions through the porous matrix is analyzed by computing their diffusion coefficients. The results show that the immobilization of the Na and Cs ions is higher in the sodalite structure as their framework lacks channels and the ions are confined in small cavities, hindering their migration and possible release. Moreover, the regular 6-membered rings favor the absorption of these ions. The structural resemblance of geopolymers to the sodalite makes these materials suitable qualities for effectively capturing Cs ions, with results that are comparable to, or even better than, the analyzed zeolites. In addition, the simulations indicate that lower Si/Al ratios improve the immobilization, owing to the negative charge of tetracoordinate Al in the geopolymer structure. All in all, this work offers a first quantitative explanation of the immobilization mechanisms of Cs in geopolymers, including their dependence on the structural disorder and chemical composition.

2. Methodology & simulation details

2.1. Model construction

For the geopolymer models, we considered four Si/Al ratios, 1.4, 1.6, 1.8, and 2.0, and three different levels of disorder: fully crystalline, fully amorphous, and a defective structure intermediate between the previous two. These models were built following the procedure summarized below and described in detail by Lolli et al. [53], whose work includes exhaustive mechanical and structural characterization to validate them. The initial structures were all built considering only silicate tetrahedra—no Al, water, nor counterions. The crystalline model is based on the geometry of sodalite, making its structure equivalent to that of zeolite. Sodalite is also the starting point for the development of the defective model. Nevertheless, for creating the defective structure, vacancies or defects were introduced by randomly deleting some silicates and rearranging the structure near the new vacancies and by rearranging the structure near the new vacancies to restore Q^4 polymerization. This results in a non-crystalline structure that retains some short-range structural order, as observed experimentally [58–60]. For the amorphous model, the baseline structure was taken from the silica glass in Sheikholeslam et al. [61]. In all cases, Q^4 polymerization has been fulfilled in agreement with the experimental data [53]. After performing energy minimization at 0 K and 1 atm, the chemistry of these baseline structures was modified by substituting some Si^{4+} with Al^{3+} to reach the target Si/Al ratios. The charge imbalance created by these substitutions was compensated by adding Na atoms at random locations, using a geometry-based algorithm [62]. Water molecules were also added at the same time to keep a H_2O/(Si+Al) ratio of 1.25. This ratio is slightly greater than the critical threshold of structural water found by Kuenzel et al., below which the material will undergo extensive shrinkage deformations [63–65].

The zeolites models were built using a similar procedure to that of the crystalline geopolymer model described above [53]. The baseline crystalline structures of chabazite [66], mordenite [67], and clinoptilolite [68] were obtained from the *Database of Zeolite Structures* [69]. The respective all-siliceous zeolitic structures were taken as a starting point and modified in several steps to impose the target Si/Al ratios and water content. Considering these structures is advantageous because they feature 8-membered rings, where the adsorption and retention of Cs are expected to be more favorable than in the 4- and 6-membered rings of the crystalline geopolymer model.

Once the models were ready, we inserted Cs ions into the porous structure of the geopolymer. To maintain the electroneutrality of the system, the sum of Cs and Na ions must equal the total number of Al, so Na was partially replaced by Cs ions, imposing a Cs/Na ratio of 0.5. To ensure a thermodynamically favorable distribution of Cs and Na ions in the porous structure, the atom swap Monte Carlo method was used. This technique enables to swap an atom of a given type with atoms of another type, in this case, Na and Cs. The swap probabilities are dictated by the temperature and chemical potential of the swap types, following the Metropolis criterion to decide whether to accept the move or to revert back to the previous configuration based on the change in the energy of the resulting state compared to the initial one [70]. The velocities of the swapped cations are scaled by the ratio of their masses to ensure that the kinetic energy of each cation is the same before and after the swap, even though the atom masses have changed. The atoms to be tentatively swapped are chosen randomly with equal probability among the

candidate atoms. In this work, we attempted 10 swaps between Cs and Na atoms every 50 fs during 0.5 ns in the canonical ensemble (NVT). To preserve the assigned Cs-Na fraction of 0.5, Cs atoms were only allowed to swap with Na atoms and vice versa.

2.2. Simulation details

All the molecular dynamics (MD) simulations were performed using the simulation code LAMMPS [71] (21-Jan-2020 version). The geopolymer models were equilibrated using the reactive force field ReaxFF [72,73], as this reactive force field is flexible enough to describe both ordered and disordered structures [74]. These simulations required a set of Si/O/H [75] and Al/O/H [76] parameters and the parameterization of the angle Si-O-Al from ref. [77] was also considered. The parametrization for Cs ions is included in the set developed by Fedkin et al. [78]. The equilibration scheme employed for the models is described in detail in ref. [53]. Essentially, it consists of performing energy minimization, followed by molecular dynamics simulations in the isobaric-isothermal (NPT) ensemble at room conditions (300 K and 1 atm) for 1 ns, followed by further relaxation in the canonical (NVT) ensemble for another 1 ns at 300 K. Finally, we run molecular dynamics (MD) simulations in the canonical ensemble (NVT) at 300 K for 5 ns, using a time step of 0.5 fs and a thermostat coupling constant of 0.1 ps to record the trajectory and properties of the systems. The analysis of the trajectory includes the calculation of coordination numbers and diffusion coefficients of the Na and Cs by computing the radial distribution functions and mean square displacements, the estimation of their adsorption enthalpies, and the lifetime of the Na-O and Cs-O pairs by means of the autocorrelation functions. These analyses are described in detail in the Supplementary Information (S.I.).

3. Results and discussion

3.1. Geopolymers

3.1.1. Coordination shells

The coordination shells of Na and Cs ions to oxygen atoms from the geopolymer aluminosilicate structure (Os) and from the water molecules (Ow) were analyzed for different degrees of crystallinity and Si/Al ratios. This analysis aimed to determine if the ions are adsorbed on the surface of the geopolymer or only solvated by the solvent. To achieve this, we computed the radial distribution functions (RDFs) and coordination numbers (CNs) of Cs and Na to those oxygen atoms. The RDF gives the probability of finding atoms of a desired type (Os or Ow) as a function of the distance from the reference atom (Cs or Na), while the CN counts the number of neighboring atoms of a given type that can be found within a defined distance. The first solvation shell corresponds to the first minimum of the RDF. More details can be found in the Supplementary Information (S.I.).

Fig. 1 illustrates the RDFs and CNs for Na and Cs ions to the oxygen atoms from water molecules (Ow) and oxygen atoms from geopolymers (Os) with different degrees of disorder and a Si/Al ratio of 1.4. Similar results were found for other Si/Al ratios, as shown in Figs. S1 and S2 of the S.I., since this ratio does not significantly alter RDFs or CNs of Na and Cs ions. In contrast, the degree of disorder matters, and Fig. 1 shows considerable differences in the peaks of RDFs, especially between the crystalline model and the other two models, although the position of these peaks remains unaltered in all models. These positions quantify the M-O distances (M is a general term to indicate either Na or Cs). The Na-O and Cs-O distances, both for water and oxygen from geopolymers, are around 2.3–2.4 Å and 3.1–3.3 Å, respectively, in agreement with Na-O and Cs-O distances from other experimental and computational studies, which ranged between 2.3 and 2.5 Å [79,80] and 3.0–3.3 Å [80–82]. Na-O distances are generally smaller than Cs-O distances because Na is smaller in size, with an ionic radius of 1.02 Å [83] as opposed to the 1.67 Å ionic radius of Cs^+ [83]. Since both cations are monovalent, this size difference results in a charge density, defined as the charge/volume ratio, much higher for Na than for Cs. The charge density affects the width and intensity of the peaks in the RDF: higher charge density leads to stronger M-O electrostatic interactions, and their peaks in the RDF tend to be sharper and more pronounced, while lower charge density can result in broader peaks with reduced intensity. This is reflected in Fig. 1, where the peaks of the RDF for Na-O pairs are slightly sharper than the corresponding peaks for Cs-O, especially for M-Os peaks.

Fig. 1 also shows the coordination numbers as a function of the distance (dashed lines), which are the integral of the RDFs. Table 1 summarizes CNs for the first neighbors of Na ions, i.e. integrating until the whole first peak and stopping at the first local minimum of the RDF between the first and the second peak (~3.1 Å for Na-Ow and ~2.8 Å for Na-Os). Table 1 only shows the CNs for Na ions for the three levels of structural disorder with Si/Al ratios of 1.4 since this ratio does not significantly affect the CNs, but the structural disorder does. In the crystalline model, Na ions are coordinated on average to about 3.5 water

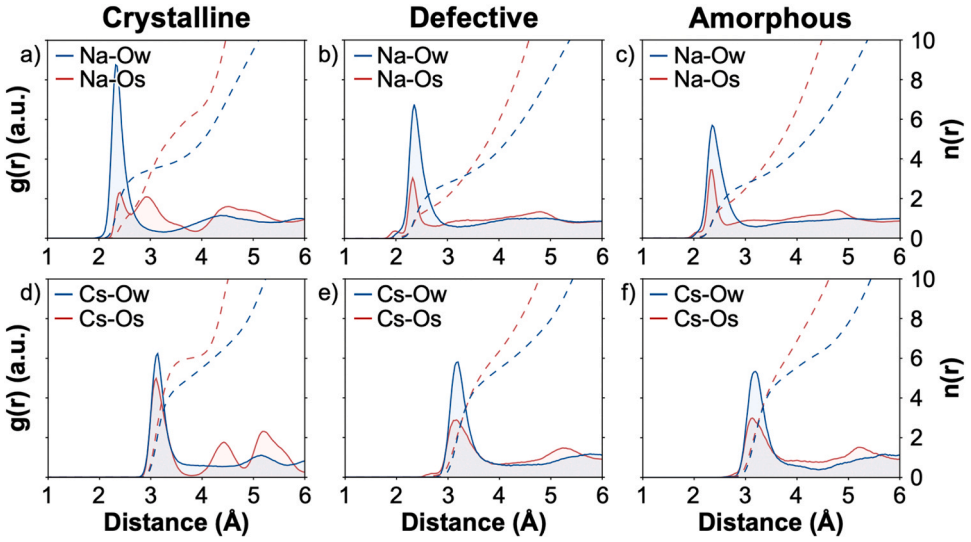

Fig. 1. RDFs (continuous lines) and CNs (dashed lines) of (a, b, c) Na and (d, e, f) Cs ions to oxygen atoms from water molecules Ow (in blue) and from the geopolymer's surface Os (in red) for the (a, d) crystalline, (b, e) defective, and (c, f) amorphous models with a Si/Al ratio of 1.4. Results for other Si/Al ratios are very similar and hence are only shown in the S.I.

Table 1
Average coordination numbers for Na to water (Ow) and oxygen atoms of the surface (Os) of the geopolymers with a Si/Al ratio of 1.4 for the different levels of disorder.

CN	Crystalline	Defective	Amorphous
Na-Ow	3.5	3.1	3.0
Na-Os	2.2	1.9	2.1
Total	**5.7**	**5.0**	**5.1**

molecules, higher than the amount observed in the defective and amorphous models, with average CNs of 3.1 and 3.0, respectively. This may be attributed to steric constraints in the non-crystalline models since, although the 3 models have a similar density, their pore structure is different; in particular, the crystalline structure features significantly larger pores than the non-crystalline models [53]. These larger pores provide room for the water molecules to surround and coordinate with the Na ions in the crystalline model.

Table 1 also shows that the coordination of Na ions to Os is similar in all cases, despite differences in composition and structural order. It is known that Na ions, due to their size, tend to be located near the center of the 6-membered rings to maximize their coordination with the forming oxygens [84,85]. These rings are present in all the structures and their RDFs exhibit a first peak at 2.3–2.4 Å corresponding to the bonding of Na ions to 2 oxygen atoms of tetrahedra forming 120° angles, which persists at all disorder levels [53]. The crystalline however shows a nearby secondary peak (~3 Å) which accounts for the other 4 neighboring Os of the 6-membered ring, bringing the total to 6 (see Fig. 1**a**, where the CN bends a bit around 6 neighbors). This secondary peak only appears in the crystalline system and it is due to the fact that in its structure, the 6-membered rings are regular, with the Si tetrahedra forming 120º angles. The split peak of Na ions in regular 6-membered rings is due to the size of the Na ions, which prevents them from coordinating simultaneously with the 6 oxygen atoms in the ring. Although not directly bonded to them, these oxygen atoms can contribute to improve the stability of the Na atoms embedded in the ring. In non-crystalline systems, the distortion of the 6-membered causes the contribution of the other members of the ring to be lost and the absence of the secondary peak at ~3 Å.

The values of the CNs for Na-Os in Table 1 are close, but not exactly 2 because there are also other positions in the geopolymer that Na ions can occupy (see Fig. 2), albeit probably less energetically favorable. These include Na ions placed (i) near the center of a 6-membered ring, but displaced towards the cavity (i.e. the center of a sodalite cell), and (ii) to

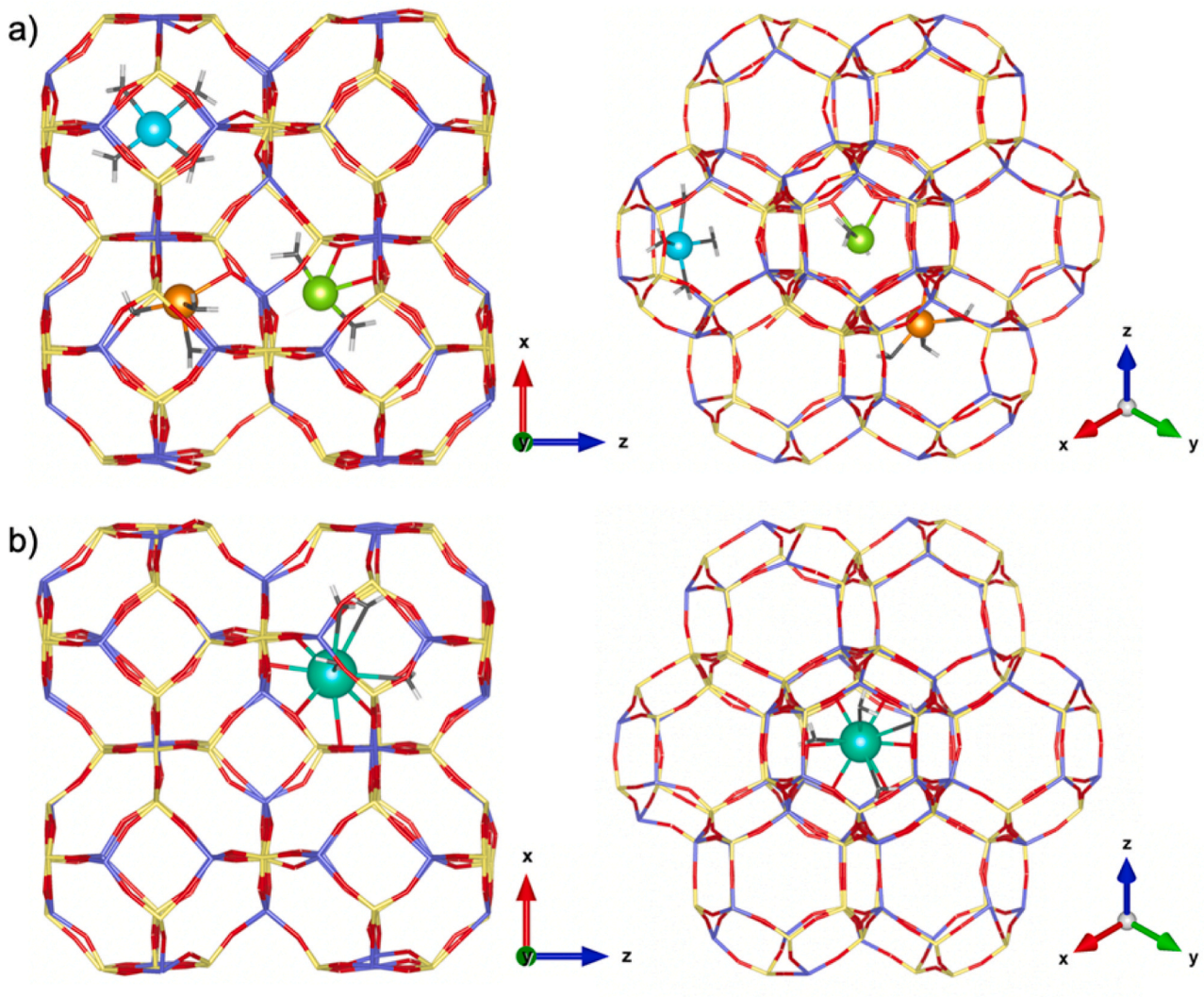

Fig. 2. Positions of (a) Na and (b) Cs in the crystalline structure of the geopolymer. Green, orange, and blue spheres in (a) represent Na ions near the center of a 6-membered ring, in a six-membered ring displaced towards the cavity at the center of a sodalite cell, and in the center of the cavity, respectively. In (b), the turquoise sphere represents a Cs ion near the center of a six-membered ring displaced towards the cavity. The structure of the geopolymer is represented by sticks in yellow, purple, and red which correspond to the bonds formed between Si, Al, and O atoms. Water molecules coordinated to the ions are illustrated as black and white sticks.

a lesser extent, in the center of the cavity. In the first scenario, the coordination to oxygen atoms of the ring is lower (1−2) than when they are not displaced into the cavity, but their coordination with water molecules increases up to 3. Finally, the solvation sphere of Na ions located in the center of the cavities is formed only by water molecules (~5). The table shows also the sum of the first peak, which is in line with the experimental and simulated values reported in the literature for Na in bulk water, between 4.0 and 6.0 [86,87].

The coordination numbers of the first-neighbor shell for Cs ions are shown in Table 2, using a threshold of ~3.7 Å; this threshold emerges clearly in the crystalline structure (Fig. 1**d**) as a minimum of the RDF after the first peak. For the disordered and amorphous structures, instead, the RDFs do not display such minimum, due to the low charge density of Cs ions. Because of the large size of the Cs ions, they coordinate to more Ow atoms than Na: 4.6 on average (Table 2) vs, 3–3.5 for Na (Table 1). Table 2 also shows that Cs ions have higher coordination with Os than with Ow, while in Na ions the opposite trend was found in Table 1. The total coordination numbers of Cs ions are between 10.2 and 10.7, in line with other values from the literature between 6.5 and 12.0 [80,82,88–91].

The maximum coordination between Cs ions and a geopolymer structure would be obtained when Cs ions sat at the center of 8-membered rings [39,41]. However, in our crystalline geopolymer model, there are no 8-membered rings and the Cs ions are accommodated near the center of the 6-membered rings, but slightly displaced towards the cavity (see Fig. 2**b**) since, given their size, they do not fit in the center of the ring. Thus, the Cs ions coordinate to 6 Os in the crystalline structure, plus to 4–5 water molecules in the cavity. The defective model has a strong structural reminiscence to the crystalline model and therefore there are enough distorted 6-membered rings where Cs ions can still be adsorbed with coordination near 6. However, those rings are slightly distorted, resulting in less effective coordination and thus a slightly lower CN of 5.7. In the structure of the defective model, besides the 6-membered rings, there are also larger rings, including 8-membered rings, where Cs ions can also be found; however, such larger rings are so much distorted that Cs ions still cannot coordinate to more than 6 Os. In the amorphous geopolymers, the coordination number of Cs to the geopolymer is also close to 6. There is no clear structural reason for this CN due to the structural complexity of this model, in which highly distorted 6- and 8-membered rings coexist with larger rings in which Cs can be accommodated, leading to an average coordination of about 6 Os oxygen atoms. For all the geopolymers, the coordination shell of Cs includes on average 4.5 water molecules.

3.1.2. *Lifetime of M-Os interactions*

Coordination alone is not a sufficient indicator of ion mobility, which also depends on interaction forces (which may be affected significantly by structural disorder) and is more directly linked to diffusion and leaching. As a first quantification of these aspects, Fig. 3 presents the autocorrelation function for Cs-Os and Na-Os pairs in the crystalline, defective, and amorphous models with a Si/Al ratio of 1.4. This function shows that the lifetime of Cs-Os pairs in the crystalline model is about 0.22 ns, while in the defective and amorphous structures, the lifetimes decrease to 0.12 and 0.09, respectively, indicating that the interaction between the Cs-Os pairs is considerably stronger in the crystalline model than in the disordered ones. The faster decay for the defective model, compared to the crystalline one, is consistent with the lower coordination of Cs in the former from Table 2. By contrast, the amorphous structure, which has a similar CN as the crystalline one, displays an even faster decay than the defective one. This indicates that structural distortions indeed may significantly impact interaction energies and therefore ion diffusion in these structures. The same trend from crystalline to defective to amorphous is also shown by the Na-Os autocorrelation functions. However, in this case, the differences induced by the structural disorder are significantly smaller: the lifetime of Na-Os interactions in the crystalline model (0.06 ns) is slightly higher than in the defective and amorphous ones (0.04 ns). Na relies mostly on interactions with only 3 Os in the 120º local arrangement, and this does not change much with disorder, hence a smaller impact of the latter.

The analysis of autocorrelation functions for different Si/Al ratios, shown in Fig. 4, reveals that, regardless of the level of disorder, the lifetime increases as the Si/Al ratio decreases. This indicates that the strength of the interactions between cations (both Cs and Na) and Os atoms increases at lower Si/Al ratios, as expected given the negative charge of tetracoordinated Al atoms.

Table 2
Average coordination numbers (CNs) for Cs to water (Ow) and oxygen atoms of the surface (Os) of the geopolymers with a Si/Al ratio of 1.4 for the different levels of disorder.

CN	Crystalline	Defective	Amorphous
Cs-Ow	4.7	4.5	4.7
Cs-Os	6.0	5.7	5.9
Total	**10.7**	**10.2**	**10.6**

3.1.3. *Diffusion coefficients*

The autocorrelation function is linked to the diffusivity of cations interacting with the Os atoms. However, some Cs and Na ions are not linked to Os and therefore their diffusivities are not controlled by the autocorrelation functions. To determine the average diffusivity of all Cs and Na ions, as well as water molecules, we have computed the diffusion coefficients from the mean square displacements of these species as explained in the S.I. Fig. 5 shows the average diffusion coefficients for Cs, Na, and water confined in the geopolymers, for the considered Si/Al ratios and degrees of order. The occlusion of these species in the close cavities of the geopolymers reduces the migration and results in values of the diffusion coefficients up to three orders of magnitude lower than in laminar materials, such as clay minerals [92–94] or C-(A)-S-H gel [95,96], and in bulk water [97]. This confirms the potential of geopolymers for Cs immobilization.

Despite the diffusion coefficients being small, Fig. 5 clearly shows that all the diffusivities increase with the Si/Al ratio. High Si/Al ratios imply fewer tetracoordinated Al in the geopolymer structure, whose negative charge contributes to binding the cations. This directly explains why the diffusivity of the cations is higher at high Si/Al ratios, but this also affects similarly the mobility of water molecules, as many of them are part of the solvation shells of the cations. Fig. 5 also shows that the diffusion coefficients in the defective and amorphous structures are quite similar and considerably higher than those of the crystalline model. This agrees with the reduction of the decay time with the disorder from the autocorrelation functions and with the interpretation that distortions in the solid skeleton cause ions to sit in energetically less favorable configurations, which in turn favors their motion and diffusion. Interestingly, the crystalline model leads to the lowest diffusion coefficients, despite its pore sizes being considerably larger than in the defective and amorphous structures [53]. This corroborates the interpretation that mobility is not controlled by steric constraints (pore sizes) as much as by how favorable the energy state of the cations is in the system and how that depends on distortions in the geopolymer structure. Finally, the lower diffusion coefficients of Cs compared to Na are consistent with their higher coordination with Os and the longer lifetime of the Cs-Os interactions.

3.2. *Adsorption enthalpies*

The previous sections have highlighted that interaction energy and its dependence on structural disorder are determining factors for cation diffusion in geopolymer structures. A direct evaluation of such energy states is done here by evaluating the adsorption enthalpies, as explained in the S.I. Table 3 presents the adsorption enthalpies for Cs and Na ions embedded in each geopolymer model. The values for Cs ions are more

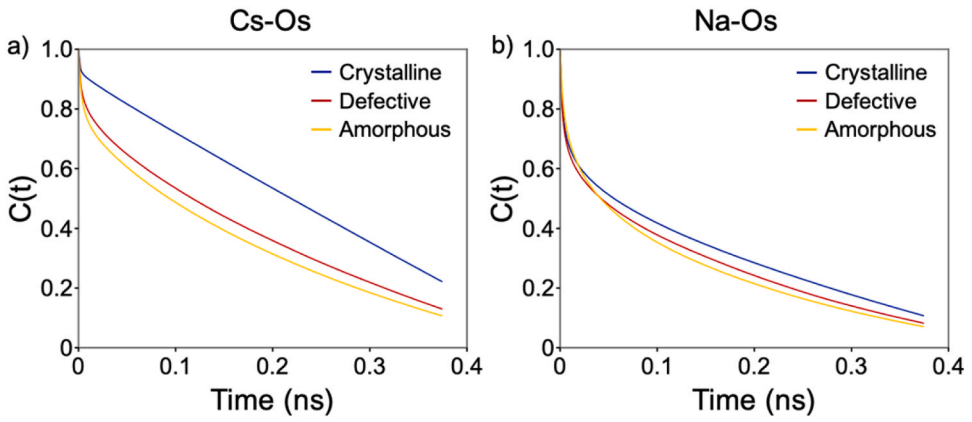

Fig. 3. Autocorrelation functions of (a) Cs–Os and, (b) Na–Os pairs in the crystalline (blue), defective (red), and amorphous (yellow) geopolymers with SiAl = 1.4.

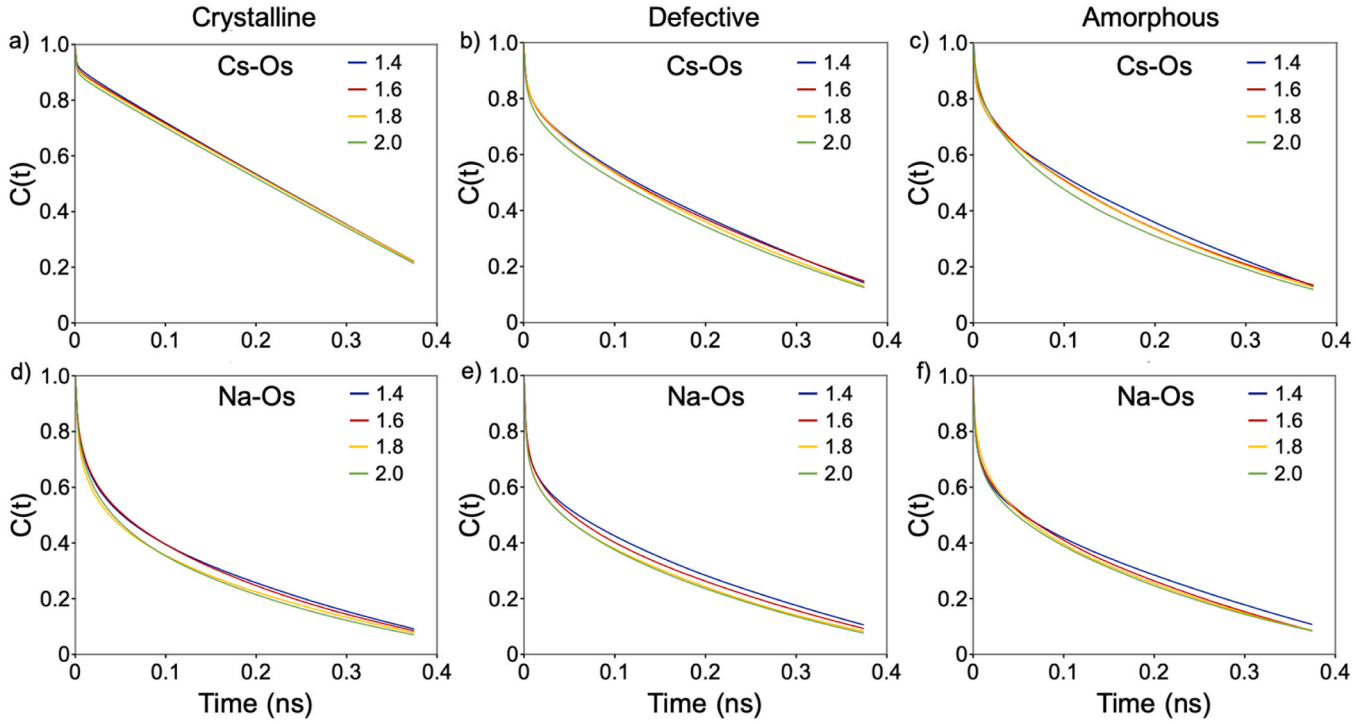

Fig. 4. Autocorrelation functions of (a-c) Cs–Os and, (d-f) Na–Os pairs in the (a, d) crystalline, (b, e) defective, and (c, f) amorphous geopolymers with SiAl = 1.4 (in blue), 1.6 (in red), 1.8 (in yellow), and 2.0 (in green).

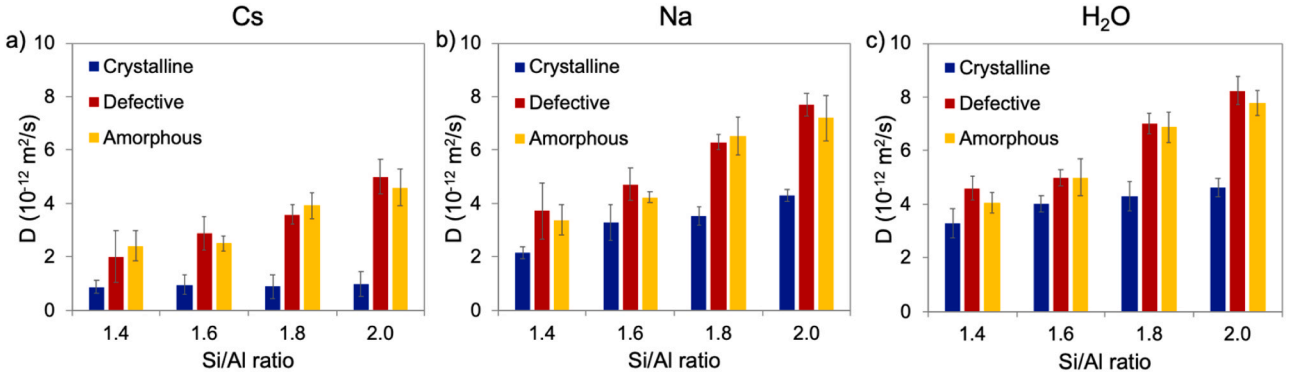

Fig. 5. Average diffusion coefficients for (a) Cs, (b) Na, and (c) water confined in the crystalline (blue), defective (red), and amorphous (yellow) geopolymers. The error bars represent the standard deviation of the diffusion coefficients from 3 independent trajectories.

Table 3
Adsorption enthalpies of Na and Cs confined in crystalline, defective, and amorphous geopolymers at the analyzed Si/Al ratios.

ΔH (kcal/mol)	Crystalline		Defective		Amorphous	
Si/Al	Na	Cs	Na	Cs	Na	Cs
1.4	-44.6	-50.6	-40.9	-46.7	-41.8	-44.8
1.6	-42.1	-48.9	-38.4	-43.5	-39.3	-44.2
1.8	-41.0	-47.8	-35.7	-42.0	-34.8	-41.3
2.0	-39.0	-46.8	-33.7	-39.7	-33.8	-40.4

negative than for Na for all the analyzed systems. This is expected, given the larger coordination of Cs from Table 2, and it means that the adsorption of Cs in our model geopolymers is more favorable than that of Na ions. For both Na and Cs ions, adsorption is more favorable (more negative enthalpies) at low Si/Al ratios, which again is due to the negative charge of tetracoordinated Al. The calculation of the diffusivity revealed similar values for the defective and amorphous models; this is consistent with the similar enthalpies shown in Table 3. Furthermore, the lower diffusion coefficients for the crystalline geopolymer are corroborated by its lower enthalpies in Table 3.

3.3. Modified zeolites

In this section, the adsorption capacity of Na and Cs ions in crystalline zeolitic structures with high adsorption capacity and selectivity towards Cs is analyzed to compare them with that of geopolymers. In particular, four zeolites were investigated: sodalite (SOD) (whose structure is identical to that of the crystalline geopolymer model), chabazite (CHA), mordenite (MOR), and clinoptilolite (HEU). This section aims to analyze the influence of the pore structure to see how pore size and its interconnection affect the immobilization capacity of Cs ions and their diffusion through the matrix, in order to better understand how these parameters can affect geopolymers. Each zeolite has a unique structure that consists of interconnected channels and cages capable of accommodating different ions, including Cs. The selectivity for an ion is determined by the size and shape of the cavity, while the size of the channels and their connectivity play a crucial role in reducing the release of the confined Cs. The selected zeolites have excellent performance in capturing and retaining Cs ions, but they exhibit different structures, as can be seen in Fig. 6. Sodalite has small pore sizes and cavities interconnected with narrow channels (formed by 4-membered rings), which prevent the release of the confined species, especially those relatively large, such as that of Cs. The structure of chabazite exhibits larger cavities interconnected by channels formed by 6-membered rings. Finally, mordenite and clinoptilolite have much wider channels (formed by 8–12-membered rings), which might facilitate the accommodation of larger molecules and their transport through the pore structure. The analysis performed in this section encompasses the Na-O and Cs-O radial distribution functions and coordination numbers, the lifetimes of Na-O and Cs-O pairs, and the diffusion coefficients and the adsorption enthalpies of those ions confined in each zeolite.

3.3.1. Coordination shell

To analyze the local structure of the cations, Cs and Na, confined in sodalite, chabazite, mordenite, and clinoptilolite, we computed the radial distribution functions (RDF) and coordination numbers (CN) for Na and Cs to oxygen atoms from the zeolites (Os) and from water molecules (Ow). Fig. 7 shows the RDFs and CNs for the zeolites with Si/Al ratios of 1.4, revealing larger differences in the coordination spheres of Na and Cs depending on the structure of the zeolite. In contrast, the Si/Al ratio does not change substantially the RDFs and CNs, as can be seen in Figs. S3 and S4 of the S.I.

The RDFs show that the Na-Ow and Cs-Ow distances are respectively 2.3–2.4 A and 3.1–3.3 A, regardless of the zeolite structure; these are in line with values from other authors, of about 2.3–2.5 Å for Na-O distances [79,80] and 3.0–3.3 Å for Cs-O distances [80–82]. As for the RDFs of the geopolymers shown in Fig. 1, Cs ions exhibit broader peaks than Na ions, due to their greater size and lower charge density. The greater size of Cs cations also leads to a much larger coordination sphere than Na ions, as shown by the CNs in Fig. 7. As for RDFs, the CNs of both Na and Cs ions change from one type of zeolite to another, whereas the impact of the Si/Al ratio is not significant. The differences observed between zeolites may be attributed to the different environments in which these cations can be accommodated due to the structural and porous matrix diversity of the analyzed zeolites, as shown in Fig. 8.

Table 4 summarizes the CNs of Na ions for the four zeolites with a Si/Al ratio of 1.4. As already mentioned, the coordination of Na ions is more efficient in 6-membered rings, which are present only in sodalite, and chabazite. Sodalite only features 4 and 6-membered rings and there is no channel [53], while chabazite also has 8-membered rings that form channels running through the zeolite [99]. The structure of mordenite and clinoptilolite includes 4, 5, 8, 10 (only in clinoptilolite), and 12-membered rings (only in mordenite), both with larger channels than chabazite [68,100]. The presence of regular 6-membered rings with the Si tetrahedra forming 120° angles in sodalite and chabazite leads to higher coordination of Na ions to oxygen atoms from the zeolite (2.1 on average,) than in mordenite and clinoptilolite (1.3 on average) that lack this local environment.

Table 4 also shows that the higher the coordination of Na ions to the geopolymers (Na-Os), the lower the coordination to water molecules, resulting in total coordination quite similar for all the structures. Nevertheless, those coordination numbers are the average for all the Na ions that can be found in different local environments. The local environments of Na ions in sodalite are the same as for the crystalline geopolymer (see Fig. 2**a**), while in chabazite Na ions are mainly near the center of 6-membered rings (orange sphere in Fig. 8**a**); to a lesser extent, they can also be found slightly displaced towards the cavity (red sphere) coordinating with fewer oxygens in the zeolite (1−2) and completing its solvation sphere with about 4–5 water molecules. In mordenite, Na ions are distributed in the 8 or 12-membered ring-channels (see Fig. 8**b**). In the 8-membered ring-channels, Na (yellow sphere) is coordinated between 2 and 3 oxygen from these rings and 2–3 water molecules. Similarly, in the 12-membered ring-channels, Na (orange sphere) can

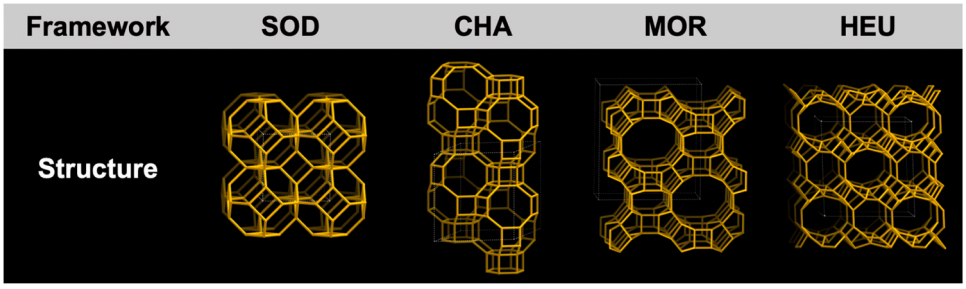

Fig. 6. Structure of sodalite (SOD), chabazite (CHA), mordenite (MOR), and clinoptilolite (HEU). The framework structures of the zeolites were obtained from *Database of Zeolite Structures* [69] and created with Jsmol software [98].

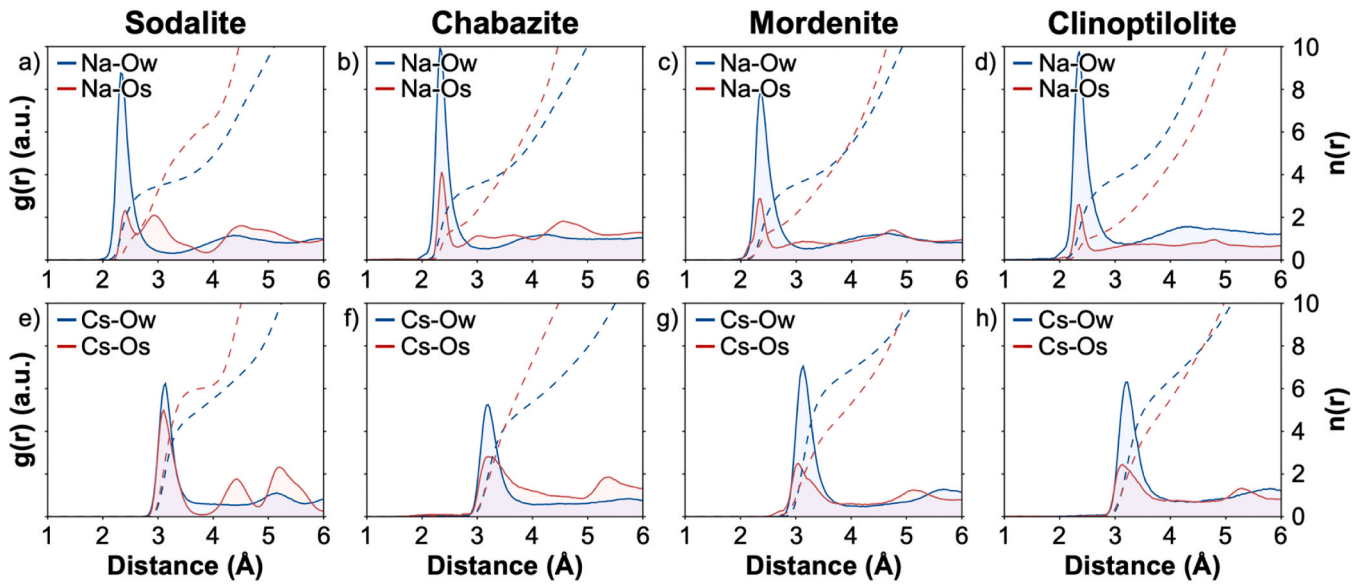

Fig. 7. RDFs (continuous lines) and CNs (dashed lines) of (a, b, c, d) Na and (e, f, g, h) Cs ions to oxygen atoms from water molecules (Os, in blue) and from the surface (Os, in red) of (a, e) sodalite, (b, f) chabazite, (c, g) mordenite, and (d, h) clinoptilolite models with a Si/Al ratio of 1.4.

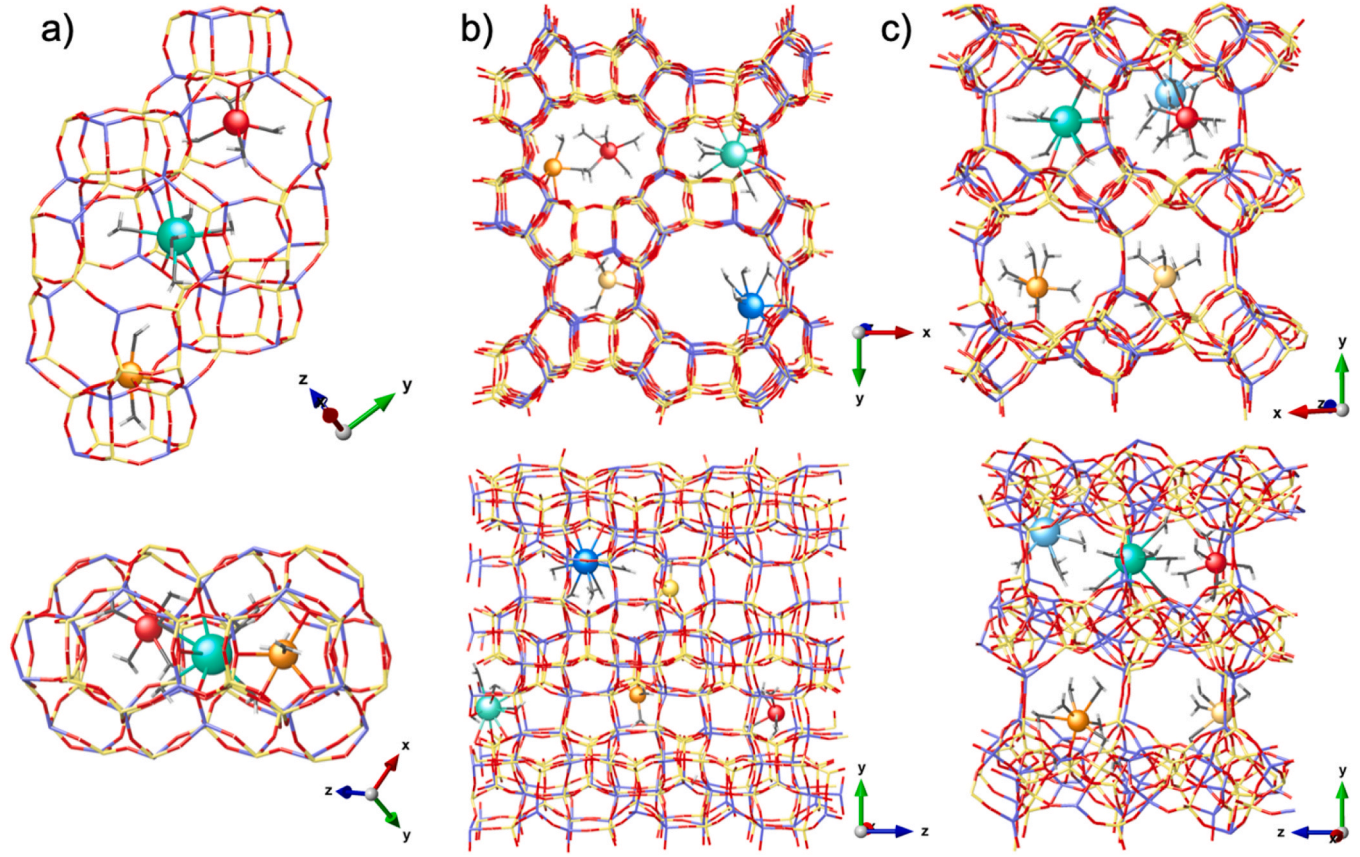

Fig. 8. Positions of Na (yellow, orange, and red spheres) and Cs (greenish-blue spheres) in (a) chabazite, (b) mordenite, and (c) clinoptilolite. The structures of the zeolites are represented by sticks in yellow, purple, and red which correspond to the bonds formed between Si, Al, and O atoms. Water is illustrated as black and white sticks. An enlarged image of the position of Na ions in the aluminosilicate rings can be seen in Fig. S5 of S.I. for better visualization.

also be coordinated to 2–3 oxygen atoms from the rings and 3–4 water molecules, but Na ions can also sit in the center of the channel, not coordinated to the rings (red sphere) and solvated by about 5–6 water molecules. Finally, clinoptilolite has open channels of 8 and 10-membered rings where Na ions can be located. There are some Na ions in the center of those channels (red sphere in Fig. 8**c**), coordinating only to water molecules (~6) or, more frequently, close to the 8 and 10-membered rings that form channels (yellow and orange spheres). These ions exhibit low coordination to the oxygen atoms of rings (1−2) and complete their coordination shell with about 2–3 water molecules.

Table 4
Average coordination numbers (CNs) for Na to water (Ow) and oxygen atoms of the surface (Os) for the different zeolites with a Si/Al ratio of 1.4.

CN	SOD	CHA	MOR	HEU
Na-Ow	3.5	3.8	4.0	4.2
Na-Os	2.2	1.9	1.4	1.2
Total	**5.7**	**5.7**	**5.4**	**5.4**

Despite the different composition of the coordination shell and the different environments in which these cations can be found, the total coordination number is similar, between 5.8 and 6.8, and in the range of the values reported in the literature, between 4.4 and 7.1 [79,80,101].

The coordination numbers for Cs confined in the analyzed zeolites with a Si/Al ratio of 1.4 are shown in Table 5. Also, in this case, the composition of the coordination sphere varies substantially depending on the type of zeolite analyzed. Cs ions tend to be located near the center of 8-membered rings to maximize the coordination to their oxygen atoms [39,41]. As with Na, Cs ions cannot coordinate to all the oxygens in the ring. Cs ions in regular 8-membered rings vibrate around the central position forming and breaking bonds continuously, coordinating on average to 6–7 oxygens simultaneously. Unlike the other 3 analyzed zeolites, sodalite does not have 8-membered rings. Thus, in sodalite Cs ions tend to sit near the center of 6-membered rings (the largest ones), although displaced towards the cavities as they do not fit in them due to their size, coordinating to the 6 oxygen atoms (see Fig. 2**b**). A higher Cs-Os coordination number, about 6–7, is found for chabazite due to the presence of 8-membered rings (turquoise sphere in Fig. 8**a**). In contrast, in the other two zeolites, the CN drops down to around 4.5. This can be attributed to the distortion of the 8-membered rings [68,99,100] in which Cs can be accommodated in mordenite and clinoptilolite (turquoise spheres in Fig. 8**b** and **c**), hampering a coordination as effective as in chabazite. Moreover, in mordenite and clinoptilolite, there are also large amounts of Cs in larger rings (blue spheres in Fig. 8**b** and **c**), where the coordination is much lower than in 8-membered rings. In all the cases, the Cs ions complete their solvation shells with about 6 water molecules in mordenite and clinoptilolite and about one less in chabazite due to the higher coordination to oxygen atoms from the zeolite, as shown in Table 5. This results in total coordination numbers between 10.4 and 10.9, in the upper range of values reported in the literature, between 6.5 and 12.0 [80,82,88–91,101].

3.3.2. *Lifetime of M-Os interactions*

Fig. 9 shows the autocorrelation functions for Cs-Os and Na-Os pairs, which provide the lifetime of the bonds between Cs and Na and the oxygen atoms (Os) from the surface of the analyzed zeolites. As for the geopolymer analyzed previously, the difference in the lifetimes from one zeolite structure to another is larger for the Cs-Os pair than for the Na-Os pairs, which indicates that Cs is bound more firmly than Na to the zeolite structures. Sodalite has a significantly higher Cs-Os lifetime, 0.22 ns, followed by chabazite (0.13 ns), clinoptilolite (0.09 ns), and mordenite (0.05 ns). The lower lifetime in chabazite compared to sodalite is not intuitive, since the cations in chabazite feature higher coordination numbers with Os atoms as per Tables 4 and 5. This may be because the Cs in sodalite can coordinate simultaneously to all 6 oxygens in the 6-membered rings and preserve those links over time, whereas in the larger 8-membered rings of chabazite, the Cs ions vibrating around the center of 8-membered rings, continuously breaking and forming bonds with the oxygen atoms of the ring. In the other two zeolites, the rings with 8 and more members are generally distorted, which hampers the coordination and reduces the Cs-Os lifetime.

The lifetime of the Na-Os pairs of chabazite (0.05 ns) is similar to that of sodalite since both have similar local structures with tetrahedra forming angles of 120°. The absence of these angles in clinoptilolite and mordenite might be responsible for Na-Os lifetimes being half as high as the values of the previous zeolites, suggesting that the adsorption sites are less stable in these zeolites.

Table 5
Average coordination numbers (CNs) for Cs to water (Ow) and oxygen atoms of the surface (Os) for the different zeolites with a Si/Al ratio of 1.4.

CN	SOD	CHA	MOR	HEU
Cs-Ow	4.7	4.5	6.2	5.7
Cs-Os	6.0	6.4	4.5	4.7
Total	**10.7**	**10.9**	**10.7**	**10.4**

3.3.3. *Diffusion coefficients*

Fig. 10 shows the diffusion coefficients for Cs, Na, and water in the analyzed zeolites at the considered Si/Al ratios. The stronger electrostatic confinement in structures with higher Al content reduces the mobility of the confined species in all the zeolites at low Si/Al ratios. Similar to the trend observed in the geopolymers, the diffusion coefficients of Cs ions are lower than those of Na ions, while water molecules have the highest diffusivity.

Fig. 10 also reveals considerable differences in the average diffusion coefficients for Cs, Na, and water molecules depending on the analyzed zeolite. The lowest values are for the species confined in sodalite, followed by those within chabazite, while the largest values are in clinoptilolite. Thus, the presence of 8, 10, and/or 12-membered ring-channels in chabazite, mordenite, and clinoptilolite enables water molecules, and also cations, to move more easily through the zeolite matrix, resulting in larger diffusion coefficients than in sodalite. Furthermore, the larger lifetimes of the M-Os pairs and the absence of channels in sodalite result in lower diffusion coefficients of both cations and water compared to chabazite, despite the ions having similar coordination numbers in the two structures. Mordenite and clinoptilolite exhibit larger diffusion coefficients, which can be related to the lower coordination of the ions to the zeolites and the lower lifetime of M-Os interactions regarding those of sodalite and chabazite.

3.3.4. *Adsorption enthalpies*

Table 6 displays the adsorption enthalpies for Cs and Na confined in sodalite, chabazite, mordenite, and clinoptilolite with Si/Al ratios between 1.4 and 2.0. The data reveal that, also here, the adsorption of both Na and Cs is more favorable (more negative values) at low Si/Al ratios. Furthermore, the adsorption of Cs ions is more favorable than the adsorption of Na, in line with the trend found in geopolymers.

Regarding the differences between zeolites, the adsorption of Na ions is more favorable in sodalite than in other zeolites. However, for Cs ions, the adsorption enthalpies in chabazite are comparable to or even more favorable than those in sodalite, which is probably due to the presence of regular 8-membered rings in chabazite. Nevertheless, Cs ions have lower diffusion coefficients in sodalite than in chabazite. This can be explained by the presence of channels in the latter and the fact that the only way for Cs to diffuse in sodalite is to jump through either a 4 or a 6-membered ring, which are very narrow for a Cs atom. Thus, although Cs is less energetically bound to the sodalite, in practice its jumping from one cavity to another cavity requires overcoming a higher energy barrier than that needed to escape from an 8-membered ring in chabazite and the diffuse through its channels. On the other hand, mordenite and clinoptilolite have adsorption enthalpies in between those of defective and amorphous geopolymer models, while their diffusion coefficients of Cs and Na are significantly higher, probably due to the presence of large channels in the structure on the zeolites.

4. Summary and conclusions

This work explored some fundamental features of the interaction between radionuclides and the molecular structure of geopolymers, to support the promise of these materials as possible solutions for the immobilization of radioactive waste. To this end, we compared various

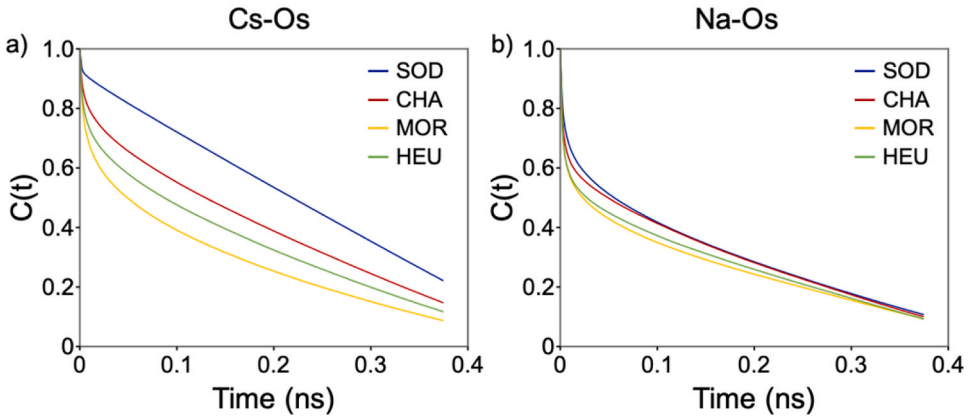

Fig. 9. Autocorrelation functions of (a) Cs–Os and, (b) Na–Os pairs in sodalite (blue), chabazite (red), mordenite (yellow), and clinoptilolite (green).

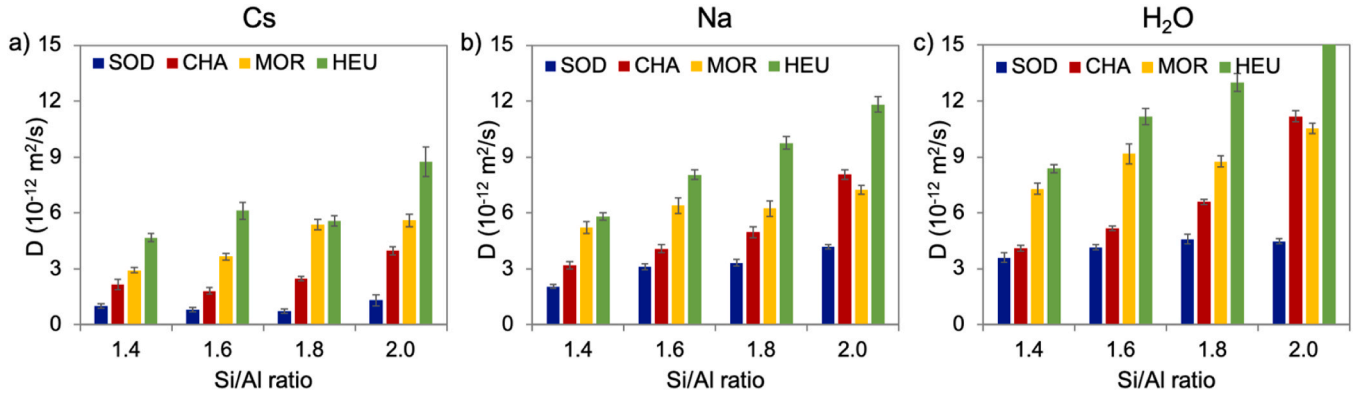

Fig. 10. Average diffusion coefficients for Cs, Na, and water confined in the analyzed zeolites.

Table 6
Adsorption enthalpies of Na and Cs confined in sodalite, mordenite, chabazite, and clinoptilolite with Si/Al ratios of 1.4, 1.6, 1.8, and 2.0.

ΔH (kcal/mol)	Sodalite		Chabazite		Mordenite		Clinoptilolite	
Si/Al	Na	Cs	Na	Cs	Na	Cs	Na	Cs
1.4	-44.7	-50.6	-36.3	-51.0	-26.7	-44.8	-34.5	-45.3
1.6	-42.3	-46.5	-33.0	-48.6	-28.2	-43.4	-30.9	-43.9
1.8	-40.2	-45.1	-31.3	-47.3	-27.7	-43.2	-28.4	-42.8
2.0	-38.5	-43.8	-24.8	-44.8	-27.3	-42.7	-26.8	-42.9

aspects of the interaction between geopolymers and Cs and Na ions in structures with various degrees of crystallinity and Si/Al ratios, and we compared them to analogous interactions in other types of crystalline zeolites (chabazite, mordenite, and clinoptilolite) with same compositions.

The local structure in which Na and Cs ions can be confined depends on the degree of crystallinity. Na ions prefer local structures with 120° angular order found in regular 6-membered rings, while Cs ions favor the center of 8-membered rings due to its larger size. In crystalline geopolymers, both Na and Cs ions tend to be located in 6-membered rings to maximize their coordination with the solid. However, in defective and amorphous models, Cs ions can be found in larger rings (mainly 8-membered rings). Despite this, the coordination is similar to that found in the crystalline geopolymers due to the distortion of the rings in the latter models. The stability of Cs-Os interactions is higher in the crystalline model, while the diffusion coefficients and adsorption enthalpies are lower, indicating that more stable configurations can be found in this model than in the defective and amorphous models. The Si/Al ratio has a clear impact on diffusivities and adsorption enthalpies, with lower values as the ratio decreases, due to higher electrostatic interactions between the positively charged ions and the more negatively charged geopolymer caused by the higher substitution of Si^{4+} by Al^{3+}.

Na ions in sodalite and chabazite have higher coordination to oxygen from the zeolites than those in mordenite and clinoptilolite due to the lack of 120° local arrangement in the latter. For Cs ions, the coordination to oxygen atoms from the zeolite is much higher in chabazite due to the presence of regular 8-membered rings, although the lifetime of Cs-Os interactions is considerably higher in sodalite since Cs ions in 6-membered rings are coordinated simultaneously to all the oxygen atoms and preserve those links over time, while in 8-membered rings Cs cannot coordinate simultaneously all the oxygen atoms of the rings, vibrating in the center of the ring forming and breaking bonds continuously. This results in lower diffusivities for ions in sodalite than in chabazite, while higher diffusivities and adsorption enthalpies are recorded for mordenite and clinoptilolite, which also decrease as the Al content rises.

Molecular dynamics simulations show that sodalite structure is best for the immobilization of Na and Cs ions due to the absence of channels and the small rings that form its structure. This hinders the migration of these ions and trapped them in their cavities. The defective geopolymer model, the closest to the real structure of geopolymers, retains certain features of the sodalite structure, and that results in favorable characteristics for the effective immobilization of Cs. Although the retention capacity of the defective geopolymer is not as strong as that of the crystalline geopolymer (equivalent to sodalite), it is comparable and, in some cases, even superior to the other analyzed zeolites, all of which exhibit excellent performance in capturing and retaining Cs ions. Moreover, the increase of the Al content considerably contributes to create more stable configurations for Cs ions in geopolymers and

zeolites, resulting in better adsorption enthalpies and lower diffusion coefficients.

Declaration of Competing Interest

The authors declare that they have no known competing financial interests or personal relationships that could have appeared to influence the work reported in this paper.

Data Availability

No data was used for the research described in the article.

Acknowledgments

This research has been funded by "Departamento de Educación, Política Lingüística y Cultura del Gobierno Vasco" through the IT1639-22 project. E.D.-R. acknowledges the postdoctoral fellowship from "Programa Posdoctoral de Perfeccionamiento de Personal Investigador Doctor" of the Basque Government. We gratefully acknowledge the technical and human support provided by i2basque and SGIker (UPV/EHU/ ERDF, EU), for the allocation of computational resources provided by the Scientific Computing Service.

Appendix A. Supporting information

Supplementary data associated with this article can be found in the online version at doi:10.1016/j.mtcomm.2023.106496.

References

[1] T.R. Naik, Sustainability of concrete construction, Pract. Period. Struct. Des. Constr. 13 (2) (2008) 98–103.
[2] S.A. Miller, A. Horvath, P.J.M. Monteiro, Readily implementable techniques can cut annual CO_2 emissions from the production of concrete by over 20%, Environ. Res. Lett. 11 (7) (2016) 74029.
[3] Nature, Concrete needs to lose its colossal carbon footprint, Nature 597 (2021) 593–594.
[4] J.L. Provis, A. Palomo, C. Shi, Advances in understanding alkali-activated materials, Cem. Concr. Res. 78 (2015) 110–125.
[5] F. Cassagnabère, M. Mouret, G. Escadeillas, P. Broilliard, A. Bertrand, Metakaolin, a solution for the precast industry to limit the clinker content in concrete: mechanical aspects, Constr. Build. Mater. 24 (7) (2010) 1109–1118.
[6] R.J. Thomas, S. Peethamparan, Alkali-activated concrete: engineering properties and stress–strain behavior, Constr. Build. Mater. 93 (2015) 49–56.
[7] T. Bakharev, Durability of geopolymer materials in sodium and magnesium sulfate solutions, Cem. Concr. Res. 35 (6) (2005) 1233–1246.
[8] V. Sata, A. Sathonsaowaphak, P. Chindaprasirt, Resistance of lignite bottom ash geopolymer mortar to sulfate and sulfuric acid attack, Cem. Concr. Compos. 34 (5) (2012) 700–708.
[9] P. Duxson, A. Fernández-Jiménez, J.L. Provis, G.C. Lukey, A. Palomo, J.S.J. van Deventer, Geopolymer technology: the current state of the art, J. Mater. Sci. 42 (9) (2007) 2917–2933.
[10] J.L. Provis, J.S.J. Van Deventer, Alkali Activated Materials: State-of-the-Art Report, RILEM TC 224-AAM, Vol. 13, Springer Science & Business Media, 2013.
[11] B. Singh, G. Ishwarya, M. Gupta, S.K. Bhattacharyya, Geopolymer concrete: a review of some recent developments, Constr. Build. Mater. 85 (2015) 78–90.
[12] Q. Tian, S. Nakama, K. Sasaki, Immobilization of cesium in fly ash-silica fume based geopolymers with different Si/Al Molar ratios, Sci. Total Environ. 687 (2019) 1127–1137.
[13] J.G.S. van Jaarsveld, J.S.J. Van Deventer, Effect of the alkali metal activator on the properties of fly ash-based geopolymers, Ind. Eng. Chem. Res. 38 (10) (1999) 3932–3941.
[14] H. Xu, J.S.J. Van Deventer, Geopolymerisation of multiple minerals, Miner. Eng. 15 (12) (2002) 1131–1139.
[15] P. He, M. Wang, S. Fu, D. Jia, S. Yan, J. Yuan, J. Xu, P. Wang, Y. Zhou, Effects of Si/Al ratio on the structure and properties of metakaolin based geopolymer, Ceram. Int. 42 (13) (2016) 14416–14422.
[16] R.A. Fletcher, K.J.D. MacKenzie, C.L. Nicholson, S. Shimada, The composition range of aluminosilicate geopolymers, J. Eur. Ceram. Soc. 25 (9) (2005) 1471–1477.
[17] P. De Silva, K. Sagoe-Crenstil, V. Sirivivatnanon, Kinetics of geopolymerization: role of Al2O3 and SiO2, Cem. Concr. Res. 37 (4) (2007) 512–518.
[18] A.S. De Vargas, D.C.C. Dal Molin, A.C.F. Vilela, F.J. Da Silva, B. Pavao, H. Veit, The effects of Na2O/SiO2 molar ratio, curing temperature and age on compressive strength, morphology and microstructure of alkali-activated fly ash-based geopolymers, Cem. Concr. Compos. 33 (6) (2011) 653–660.
[19] P. Duan, C. Yan, W. Zhou, W. Luo, Thermal behavior of portland cement and fly ash–metakaolin-based geopolymer cement pastes, Arab. J. Sci. Eng. 40 (8) (2015) 2261–2269.
[20] M.A.M. Ariffin, M.A.R. Bhutta, M.W. Hussin, M.M. Tahir, N. Aziah, Sulfuric acid resistance of blended ash geopolymer concrete, Constr. Build. Mater. 43 (2013) 80–86.
[21] J.G. Jang, S.M. Park, H.-K. Lee, Physical barrier effect of geopolymeric waste form on diffusivity of cesium and strontium, J. Hazard. Mater. 318 (2016) 339–346.
[22] V. Nikolić, M. Komljenović, N. Marjanović, Z. Baščarević, R. Petrović, Lead immobilization by geopolymers based on mechanically activated fly ash, Ceram. Int. 40 (6) (2014) 8479–8488.
[23] J.L. Provis, P.A. Walls, J.S.J. van Deventer, Geopolymerisation kinetics. 3. effects of Cs and Sr salts, Chem. Eng. Sci. 63 (18) (2008) 4480–4489.
[24] C. Kuenzel, J.F. Cisneros, T.P. Neville, L.J. Vandeperre, S.J.R. Simons, J. Bensted, C.R. Cheeseman, Encapsulation of Cs/Sr contaminated clinoptilolite in geopolymers produced from metakaolin, J. Nucl. Mater. 466 (2015) 94–99.
[25] M.Y. Khalil, E. Merz, Immobilization of intermediate-level wastes in geopolymers, J. Nucl. Mater. 211 (2) (1994) 141–148.
[26] A. Fernández-Jiménez, D.E. Macphee, E.E. Lachowski, A. Palomo, Immobilization of cesium in alkaline activated fly ash matrix, J. Nucl. Mater. 346 (2–3) (2005) 185–193.
[27] C. Shi, A. Fernandez-Jimenez, Stabilization/solidification of hazardous and radioactive wastes with alkali-activated cements, J. Hazard. Mater. 137 (3) (2006) 1656–1663.
[28] D.S. Perera, E.R. Vance, Z. Aly, J. Davis, C.L. Nicholson, Immobilization of Cs and Sr in geopolymers with Si/Al molar ratio Of~ 2, Ceram. Trans. 176 (2006) 91.
[29] S.A. Rasaki, Z. Bingxue, R. Guarecuco, T. Thomas, Y. Minghui, Geopolymer for use in heavy metals adsorption, and advanced oxidative processes: a critical review, J. Clean. Prod. 213 (2019) 42–58.
[30] Y. Zhu, Z. Zheng, Y. Deng, C. Shi, Z. Zhang, Advances in immobilization of radionuclide wastes by alkali activated cement and related materials, Cem. Concr. Compos. 126 (2022), 104377.
[31] Q. Tian, Y. Bai, Y. Pan, C. Chen, S. Yao, K. Sasaki, H. Zhang, Application of geopolymer in stabilization/solidification of hazardous pollutants: a review, Molecules 27 (14) (2022) 4570.
[32] S. Jain, N. Banthia, T. Troczynski, Leaching of immobilized cesium from NaOH-activated fly ash-based geopolymers, Cem. Concr. Compos. 133 (2022), 104679.
[33] E. Phillip, T.F. Choo, N.W.A. Khairuddin, On the sustainable utilization of geopolymers for safe management of radioactive waste: a review, Sustainability 15 (2) (2023) 1117.
[34] M. Hafez, A. Nazmy, F. Salem, M. Eldesoki, Fixation mechanism between zeolite and some radioactive elements, J. Radioanal. Nucl. Chem. 47 (1–2) (1978) 115–119.
[35] R. Harjula, J. Lehto, Effect of sodium and potassium ions on cesium absorption from nuclear power plant waste solutions on synthetic zeolites, Nucl. Chem. Waste Manag. 6 (2) (1986) 133–137.
[36] P.K. Sinha, P.K. Panicker, R.V. Amalraj, V. Krishnasamy, Treatment of radioactive liquid waste containing caesium by indigenously available synthetic zeolites: a comparative study, Waste Manag 15 (2) (1995) 149–157.
[37] P.K. Sinha, V. Krishnasamy, Fixation of caesium, strontium and thorium ions in commercial synthetic zeolite matrices by thermal treatment, J. Nucl. Sci. Technol. 33 (4) (1996) 333–340.
[38] E. Johan, T. Yamada, M.W. Munthali, P. Kabwadza-Corner, H. Aono, N. Matsue, Natural zeolites as potential materials for decontamination of radioactive cesium, Procedia Environ. Sci. 28 (2015) 52–56.
[39] H.Y. Lee, H.S. Kim, H.-K. Jeong, M. Park, D.-Y. Chung, K.-Y. Lee, E.-H. Lee, W. T. Lim, Selective removal of radioactive cesium from nuclear waste by zeolites: on the origin of cesium selectivity revealed by systematic crystallographic studies, J. Phys. Chem. C. 121 (19) (2017) 10594–10608.
[40] E. Han, Y.-G. Kim, H.-M. Yang, I.-H. Yoon, M. Choi, Synergy between zeolite framework and encapsulated sulfur for enhanced ion-exchange selectivity to radioactive cesium, Chem. Mater. 30 (16) (2018) 5777–5785.
[41] S. Kwon, C. Kim, E. Han, H. Lee, H.S. Cho, M. Choi, Relationship between zeolite structure and capture capability for radioactive cesium and strontium, J. Hazard. Mater. (2020), 124419.
[42] M. Jiménez-Reyes, P.T. Almazán-Sánchez, M. Solache-Ríos, Radioactive waste treatments by using zeolites. a short review, J. Environ. Radioact. 233 (2021), 106610.
[43] M.M. Kumar, K.A. Irshad, H. Jena, Removal of Cs+ and Sr2+ ions from simulated radioactive waste solutions using zeolite-A synthesized from kaolin and their structural stability at high pressures, Microporous Mesoporous Mater. 312 (2021), 110773.
[44] M. Park, S. Kim, Y. Takahashi, H.Y. Jeong, Thermal stabilization of extraframework Cs+ in zeolite 13X, J. Nucl. Mater. 572 (2022), 154078.
[45] E. Erdem, N. Karapinar, R. Donat, The removal of heavy metal cations by natural zeolites, J. Colloid Interface Sci. 280 (2) (2004) 309–314.
[46] N.N. Ilchenko, O.V. Kuchma, Y.L. Zub, J. Leszczynski, Cesium cation complexation by 25, 27-dihydroxycalix [4] arene-crown-6: computational study, J. Mol. Struct. THEOCHEM 815 (1–3) (2007) 83–86.
[47] M. Šljivić, I. Smičiklas, S. Pejanović, I. Plećaš, Comparative study of Cu2+ adsorption on a zeolite, a clay and a diatomite from Serbia, Appl. Clay Sci. 43 (1) (2009) 33–40.
[48] M.R. Awual, S. Suzuki, T. Taguchi, H. Shiwaku, Y. Okamoto, T. Yaita, Radioactive cesium removal from nuclear wastewater by novel inorganic and conjugate adsorbents, Chem. Eng. J. 242 (2014) 127–135.

[49] S. Fu, P. He, M. Wang, J. Cui, M. Wang, X. Duan, Z. Yang, D. Jia, Y. Zhou, Hydrothermal synthesis of pollucite from metakaolin-based geopolymer for hazardous wastes storage, J. Clean. Prod. 248 (2020), 119240.

[50] P. He, Q. Wang, S. Fu, M. Wang, S. Zhao, X. Liu, Y. Jiang, D. Jia, Y. Zhou, Hydrothermal transformation of geopolymers to bulk zeolite structures for efficient hazardous elements adsorption, Sci. Total Environ. 767 (2021), 144973.

[51] S. Ma, H. Yang, S. Fu, P. He, X. Duan, Z. Yang, D. Jia, P. Colombo, Y. Zhou, Additive manufacturing of geopolymers with hierarchical porosity for highly efficient removal of Cs, J. Hazard. Mater. 443 (2023), 130161.

[52] H. Nakamura, M. Okumura, M. Machida, First-principles calculation study of mechanism of cation adsorption selectivity of zeolites: a guideline for effective removal of radioactive cesium, J. Phys. Soc. Jpn. 82 (2) (2012) 23801.

[53] F. Lolli, H. Manzano, J.L. Provis, M.C. Bignozzi, E. Masoero, Atomistic simulations of geopolymer models: the impact of disorder on structure and mechanics, ACS Appl. Mater. Interfaces 10 (26) (2018) 22809–22820.

[54] E.H. Borai, R. Harjula, A. Paajanen, Efficient removal of cesium from low-level radioactive liquid waste using natural and impregnated zeolite minerals, J. Hazard. Mater. 172 (1) (2009) 416–422.

[55] T.-H. Wang, M.-H. Li, W.-C. Yeh, Y.-Y. Wei, S.-P. Teng, Removal of cesium ions from aqueous solution by adsorption onto local taiwan laterite, J. Hazard. Mater. 160 (2–3) (2008) 638–642.

[56] H.A. Ibrahim, A.M. El-Kamash, M. Hanafy, N.M. Abdel-Monem, Examination of the use of synthetic zeolite NaA–X blend as backfill material in a radioactive waste disposal facility: thermodynamic approach, Chem. Eng. J. 144 (1) (2008) 67–74.

[57] H. Mimura, T. Kanno, Distribution and fixation of cesium and strontium in zeolite A and chabazite, J. Nucl. Sci. Technol. 22 (4) (1985) 284–291.

[58] C.E. White, K. Page, N.J. Henson, J.L. Provis, In situ synchrotron X-ray pair distribution function analysis of the early stages of gel formation in metakaolin-based geopolymers, Appl. Clay Sci. 73 (2013) 17–25.

[59] W.M. Kriven, M. Gordon, J.L. Bell, Geopolymers: nanoparticulate, nanoporous ceramics made under ambient conditions, Microsc. Microanal. 10 (S02) (2004) 404–405.

[60] A. Fernández-Jiménez, M. Monzó, M. Vicent, A. Barba, A. Palomo, Alkaline activation of metakaolin–fly ash mixtures: obtain of zeoceramics and zeocements, Microporous Mesoporous Mater. 108 (1–3) (2008) 41–49.

[61] S.A. Sheikholeslam, H. Manzano, C. Grecu, A. Ivanov, Reduced hydrogen diffusion in strained amorphous SiO 2: understanding ageing in MOSFET devices, J. Mater. Chem. C. 4 (34) (2016) 8104–8110.

[62] L. Martínez, R. Andrade, E.G. Birgin, J.M. Martínez, PACKMOL: A Package for Building Initial Configurations for Molecular Dynamics Simulations, Vol. 30, Wiley Subscription Services, Inc., A Wiley Company, 2009, pp. 2157–2164.

[63] P. Duxson, G.C. Lukey, J.S.J. van Deventer, Physical evolution of Na-geopolymer derived from metakaolin up to 1000C, J. Mater. Sci. 42 (9) (2007) 3044–3054.

[64] C. Kuenzel, L.J. Vandeperre, Ambient temperature drying shrinkage and cracking in metakaolin-based geopolymers, J. Am. Ceram. Soc. 95 (10) (2012) 3270–3277.

[65] F. Lolli, J.J. Thomas, K.E. Kurtis, F. Cucinotta, E. Masoero, Early age volume changes in metakaolin geopolymers: insights from molecular simulations and experiments, Cem. Concr. Res. 144 (2021), 106428.

[66] M. Calligaris, G. Nardin, L. Randaccio, Cation site location in hydrated chabazites. crystal structure of potassium-and silver-exchanged chabazites, Zeolites 3 (3) (1983) 205–208.

[67] Gramlich, V. Phd Thesis, ETH Zurich, 1971.

[68] K. Koyama, Y. Takeuchi, Clinoptilolite: the distribution of potassium atoms and its role in thermal stability, Z. für Krist. Mater. 145 (3–4) (1977) 216–239.

[69] Baerlocher, C.; McCusker, L.B. Database of Zeolite Structures http://www.iza-structure.org/databases/ (accessed Jan 11, 2021).

[70] R.K. Pathria, P.D. Beale, 16 - computer simulations, in: R.K. Pathria, P.D. Beale (Eds.), In *Statistical Mechanics*, *Third edition*.,, Academic Press, Boston, 2011, pp. 637–652.

[71] S. Plimpton, Fast parallel algorithms for short-range molecular dynamics, J. Comput. Phys. 117 (1) (1995) 1–19.

[72] M. Russo, A.C.T. van Duin, Atomistic-scale simulations of chemical reactions: bridging from quantum chemistry to engineering, Nucl. Inst. Methods Phys. Res. B 269 (2011) 1549–1554.

[73] A.C.T. van Duin, S. Dasgupta, F. Lorant, W.A. Goddard, ReaxFF: a reactive force field for hydrocarbons, J. Phys. Chem. A 105 (41) (2001) 9396–9409.

[74] E. Duque-Redondo, P.A. Bonnaud, H. Manzano, A comprehensive review of CSH empirical and computational models, their applications, and practical aspects, Cem. Concr. Res. 156 (2022), 106784.

[75] J.C. Fogarty, H.M. Aktulga, A.Y. Grama, A.C.T. van Duin, S.A. Pandit, A reactive molecular dynamics simulation of the silica-water interface, J. Chem. Phys. 132 (17) (2010) 174704_1–174704_10.

[76] K.L. Joshi, Van Duin, Molecular dynamics study on the influence of additives on the high-temperature structural and acidic properties of ZSM-5 zeolite, Energy Fuels 27 (8) (2013) 4481–4488.

[77] K.L. Joshi, G. Psofogiannakis, Reactive molecular simulations of protonation of water clusters and depletion of acidity in H-ZSM-5 zeolite, Phys. Chem. Chem. Phys. 16 (34) (2014) 18433–18441.

[78] M.V. Fedkin, Y.K. Shin, N. Dasgupta, J. Yeon, W. Zhang, Development of the ReaxFF methodology for electrolyte–water systems, J. Phys. Chem. A 123 (10) (2019) 2125–2141.

[79] D. Bucher, L. Guidoni, P. Carloni, U. Rothlisberger, Coordination numbers of K(+) and Na(+) ions inside the selectivity filter of the KcsA potassium channel: insights from first principles molecular dynamics, Biophys. J. 98 (10) (2010) 47–49.

[80] J. Mähler, I. Persson, A study of the hydration of the alkali metal ions in aqueous solution, Inorg. Chem. 51 (1) (2011) 425–438.

[81] C.F. Schwenk, T.S. Hofer, B.M. Rode, "Structure breaking" effect of hydrated Cs, J. Phys. Chem. A 108 (9) (2004) 1509–1514.

[82] V. Mile, L. Pusztai, H. Dominguez, O. Pizio, Understanding the structure of aqueous cesium chloride solutions by combining diffraction experiments, molecular dynamics simulations, and reverse monte carlo modeling, J. Phys. Chem. B 113 (31) (2009) 10760–10769.

[83] R.D. t Revised Shannon, Effective ionic radii and systematic studies of interatomic distances in halides and chalcogenides, Acta Crystallogr. Sect. A Cryst. Phys., Diffr., Theor. Gen. Crystallogr. 32 (5) (1976) 751–767.

[84] A. Poeppl, T. Rudolf, P. Manikandan, D. Goldfarb, W-and X-band pulsed electron nuclear double-resonance study of a sodium− nitric oxide adsorption complex in NaA zeolites, J. Am. Chem. Soc. 122 (41) (2000) 10194–10200.

[85] O.M. Dzhigit, A.V. Kiselev, K.N. Mikos, G.G. Muttik, T.A. Rahmanova, Heats of adsorption of water vapour on X-zeolites containing Li+, Na+, K+, Rb+, and Cs+ cations, Trans. Faraday Soc. 67 (1971) 458–467.

[86] J. Mahler, I. Persson, A study of the hydration of the alkali metal ions in aqueous solution, Inorg. Chem. 51 (1) (2012) 425–438.

[87] C.N. Rowley, B. Roux, The solvation structure of Na+ and K+ in liquid water determined from high level Ab initio molecular dynamics simulations, J. Chem. Theory Comput. 8 (10) (2012) 3526–3535.

[88] T.S. Hofer, H.T. Tran, C.F. Schwenk, B.M. Rode, Characterization of dynamics and reactivities of solvated ions by Ab initio simulations, J. Comput. Chem. 25 (2) (2004) 211–217.

[89] C.A. Weiss, R.J. Kirkpatrick, S.P. Altaner, Variations in interlayer cation sites of clay minerals as studied by 133Cs MAS nuclear magnetic resonance spectroscopy, Am. Mineral. 75 (9–10) (1990) 970–982.

[90] I. Bérend, J.-M. Cases, M. François, J.-P. Uriot, L. Michot, A. Masion, F. Thomas, Mechanism of adsorption and desorption of water vapor by homoionic montmorillonites: 2. The Li+ Na+, K+, Rb+ and Cs+-exchanged forms, Clays Clay Min. 43 (3) (1995) 324–336.

[91] G. Kosakowski, S.V. Churakov, T. Thoenen, Diffusion of Na and Cs in montmorillonite, Clays Clay Min. 56 (2) (2008) 190–206.

[92] V. Marry, P. Turq, Microscopic simulations of interlayer structure and dynamics in bihydrated heteroionic montmorillonites, J. Phys. Chem. B 107 (8) (2003) 1832–1839.

[93] T. Kozaki, H. Sato, S. Sato, H. Ohashi, Diffusion mechanism of cesium ions in compacted montmorillonite, Eng. Geol. 54 (1) (1999) 223–230.

[94] N. Malikova, V. Marry, J.-F. Dufrêche, P. Turq, Na/Cs montmorillonite: temperature activation of diffusion by simulation, Curr. Opin. Colloid Interface Sci. 9 (1) (2004) 124–127.

[95] E. Duque-Redondo, K. Yamada, J.S. Dolado, H. Manzano, Microscopic mechanism of radionuclide Cs retention in Al containing CSH nanopores, Comput. Mater. Sci. 190 (2021), 110312.

[96] E. Duque-Redondo, K. Yamada, I. López-Arbeloa, H. Manzano, Cs-137 immobilization in C-S-H gel nanopores, Phys. Chem. Chem. Phys. 20 (14) (2018) 9289–9297.

[97] L. Yuan-Hui, S. Gregory, Diffusion of ions in sea water and in deep-sea sediments, Geochim. Cosmochim. Acta 38 (5) (1974) 703–714.

[98] R.M. Hanson, J. Prilusky, Z. Renjian, T. Nakane, J.L. Sussman, JSmol and the next-generation web-based representation of 3D molecular structure as applied to proteopedia, Isr. J. Chem. 53 (3–4) (2013) 207–216.

[99] L.S. Dent, J.V. Smith, Crystal structure of chabazite, a molecular sieve, Nature 181 (4626) (1958) 1794–1796.

[100] W. Meier, The crystal structure of mordenite (Ptilolite), Z. Krist. Mater. 115 (1–6) (1961) 439–450.

[101] N.W. Ockwig, R.T. Cygan, L.J. Criscenti, T.M. Nenoff, Molecular dynamics studies of nanoconfined water in clinoptilolite and heulandite zeolites, Phys. Chem. Chem. Phys. 10 (6) (2008) 800–807.